1. Introduction

Two-dimensional Boussinesq convection in an imposed vertical magnetic field is specified by five parameters: the Rayleigh number R, which is proportional to the temperature difference across the fluid layer; the Chandrasekhar number Q, which is a measure of the strength of the magnetic field; the viscous and magnetic Prandtl numbers (σ and ζ respectively); and the aspect ratio of the convective roll $\varpi = 4L^2/(1+L^2)$, where L is the dimensionless width of the roll [1]. The state of the fluid is described by the stream-function and by the deviations from the static temperature profile and magnetic profile. These variables are functions of time and of the two space coordinates; their evolution is governed by a set of nonlinear partial differential equations (PDEs). The problem is invariant under reflections in a vertical plane.

If the temperature difference across the layer is small, then all fluid motion will decay due to viscous damping, leaving a uniform vertical magnetic field and a linear vertical temperature gradient. If the magnetic field is small, then the initial bifurcation as R increases is a pitchfork bifurcation from this state of no motion (the trivial solution) to one of steady convection. The two nontrivial steady solutions (one with the roll turning clockwise and the other with the roll turning counter-clockwise) are related by the reflection symmetry of the problem. As Q increases, the tension in the magnetic lines of force opposes the convective motion, until Q exceeds a critical value $Q_{\rm C}$, beyond which the initial bifurcation is a Hopf (oscillatory) bifurcation. At the bifurcation point C, where $(R, Q) = (R_{\rm C}, Q_{\rm C})$, the Hopf and pitchfork bifurcations coincide, and the problem has a pair of zero eigenvalues. Thus the point C is a codimension-two Takens–Bogdanov [2, 3, 4] or ζ^2 [5] bifurcation point with reflection symmetry, and the dynamics of the fluid for (R, Q) near $(R_{\rm C}, Q_{\rm C})$ is governed by a second-order set of nonlinear ordinary differential equations (ODEs):

$$\ddot{v} = \kappa\dot{v} - \lambda v + Mv^3 + Nv^2\dot{v} + \mathcal{O}(v^5). \tag{1}$$

Here, v is the amplitude of the convective motion (the stream-function is proportional to v), and κ and λ are unfolding parameters that are zero at the point C and are linearly related to R and Q. The constants M and N depend on the physical parameters of the problem, and can be positive or negative [6].

Equation (1) was derived from the PDEs for convection in a vertical magnetic field using perturbative techniques [6]: near the codimension-two bifurcation point, the amplitude of the motion is small so a weakly nonlinear analysis is possible. Other double convection problems (for example, thermosolutal convection [6, 7], convection in a rotating layer [8] and convection in a horizontal magnetic field [9]) have Takens–Bogdanov bifurcation points and are governed by the same normal form.

If the convective rolls are forced to be very narrow ($\varpi \to 0$), the PDEs for magnetoconvection have an additional zero eigenvalue, so the dynamics on the centre manifold is governed by the third-order normal form for the $\zeta^2\zeta$ bifurcation with reflection symmetry. The complete analysis of this bifurcation point would result in an unwelcome plethora of coefficients and cases; we do not propose to treat this general case. A perturbation analysis of the PDEs with ϖ as a distinguished small parameter yields a third-order set of ODEs that describes the dynamics of the PDEs in a ϖ-neighbourhood of the point C [10, 11]:

$$\begin{aligned} \ddot{v} &= \kappa\dot{v} - \lambda v - vw + \mathcal{O}(\varpi), \\ \dot{w} &= -w + v^2 + \mathcal{O}(\varpi), \end{aligned} \tag{2}$$

where as above the stream-function is proportional to v, and w is proportional to the horizontally averaged temperature. The unfolding parameters κ and λ are zero at the point C, but are otherwise order 1 quantities. The reflection symmetry of the original problem has the effect that (2) is invariant under the substitution $(v, w) \to (-v, w)$; solutions of the equations either have this symmetry or come in pairs related by this symmetry. Since one of the three small eigenvalues in this problem

is always negative (it is proportional to $-\varpi$), it is scaled to -1; this corresponds to taking a particular two-dimensional slice through the three-dimensional unfolding space of the normal form of the $\zeta^2\zeta$ bifurcation.

The technique used to derive (2) allows the reconstruction of asymptotically exact solutions of the PDEs from the solutions of (2) with an error that goes to zero as $\varpi \to 0$ [10, 11]. It is therefore interesting to analyse (2) and work out its bifurcation structure, as this provides the bifurcation structure of the PDEs for convection in a vertical magnetic field in a neighbourhood of the point $(R_{\rm C}, Q_{\rm C})$, in the limit of narrow rolls. In particular, the existence of chaotic trajectories in (2) implies the existence of chaotic trajectories in the PDEs. Equation (2) is a valid model of the PDEs in a parameter régime where they have not been studied in detail, although this régime is physically relevant since convection in a strong vertical magnetic field does occur in narrow rolls.

Proctor and Weiss [12] have derived a related set of equations that are an asymptotically exact model of thermosolutal convection in narrow rolls in the limit of small solutal diffusivity. Although their equations differ from (2) only in the sign of the nonlinearity in the first equation, the behaviour of the nonlinear solutions is qualitatively very different. They in effect examine a different case in the unfolding of the $\zeta^2\zeta$ bifurcation. Knobloch and Weiss [13] have studied numerically a related fifth-order model of convection in a vertical magnetic field in square rolls ($\varpi = 2$), and found chaotic trajectories associated with a heteroclinic connection between a pair of saddle-foci that satisfied Shil'nikov's criterion [14]. This fifth-order model was derived from the PDEs by a Galërkin truncation [15] in the same way that the Lorenz equations were derived from the PDEs for Bénard convection [16]. As in the case of the Lorenz equations [17], the chaos in the fifth-order model has not been discovered in the PDEs [18, 19].

Equations (2) are equivalent to a set of equations put forward by Shimizu and Morioka [20] as an *ad hoc* model of the Lorenz equations in the limit of large Rayleigh number. Shimizu and Morioka considered only very large negative values of λ; this paper considers order 1 values of λ, which are of interest in the context of magnetoconvection. A.L. Shil'nikov [21, 22, 23] has also studied these equations independently.

This paper concentrates on the analysis of (2) in the parameter range $0 \geq \kappa \geq -5$ and $0 \geq \lambda \geq -30$, which corresponds to the Chandrasekhar number $Q < Q_{\rm C}$. In section 2, we start the analysis with small values of κ and λ, near the codimension-two point C. In section 3, we examine the line of gluing bifurcations, which originates at C, for $\lambda \geq -5$, and find a codimension-two bifurcation point at which the gluing bifurcation splits into a pair of homoclinic explosions. The analysis of the point has been presented by Lyubimov and Zaks [24]. In section 4, we complete our study of the region $\lambda \geq -5$, and analyse a new codimension-two bifurcation point, at which a line of subcritical period-doubling bifurcations is created. The analysis of this point has not been presented elsewhere. In section 5, we extend the numerical study to include values of λ down to -30. We conclude in section 6.

The schematic bifurcation diagrams presented in this paper will be diagonal slices though the (κ, λ) plane, with the imposed magnetic field (Q) held fixed, and with increasing Rayleigh number (R). For the purposes of qualitative comparison with the convection problem, we make the identification $R = R_{\rm C} + \kappa - \lambda$ and $Q = Q_{\rm C} + \kappa + \lambda$. The quantitative relation between (R, Q) and (κ, λ) is given by [11]. The parameter R will appear on the horizontal axis of the bifurcation diagrams, and the amplitude of the solution will appear on the vertical axis.

"Brute force" bifurcation diagrams [25] will also be used to describe the evolution of the attractors of the ODEs as one of the parameters is varied. In these calculations, we consider a return plane $w =$ constant. Periodic or chaotic trajectories of the ODEs will repeatedly intersect this plane; we will plot the coordinates of these intersections against the unfolding parameter κ.

The unfolding diagrams presented in this paper were computed using the continuation package AUTO [26]. The calculation of the local bifurcations (those that involve Floquet multipliers crossing the unit circle) is straightforward with AUTO; the homoclinic bifurcations are well approximated by following orbits of large period.

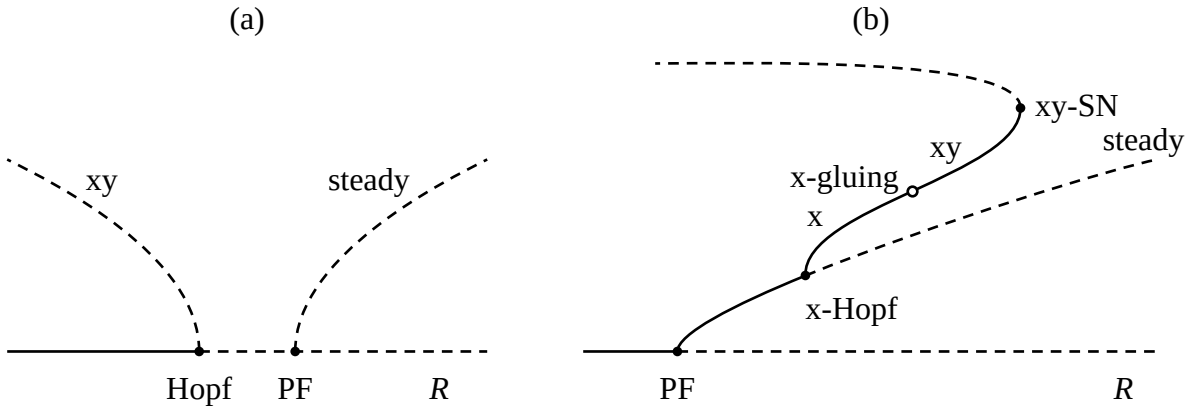

Figure 1. *Schematic bifurcation diagram for two slices through the unfolding diagram. (a) $Q > Q_{\mathrm{C}}$ ($\kappa + \lambda > 0$); (b) $Q < Q_{\mathrm{C}}$ ($\kappa + \lambda < 0$). The Rayleigh number R is on the horizontal axis and the amplitude of the solution is on the vertical axis. Solid lines represent stable solutions; dashed lines represent unstable solutions. Filled circles represent local bifurcations and open circle represent global (homoclinic) bifurcations.*

2. Vicinity of the codimension-two point C

Equation (2) has three equilibrium points: the trivial solution $(v, w) = (0, 0)$, and a symmetric pair of equilibrium points $(v, w) = (\pm\sqrt{-\lambda}, -\lambda)$, which exist only for $\lambda \leq 0$. These two non-trivial solutions correspond to steady convection in the original problem and are related by the reflection symmetry. The bifurcations from the trivial solution are a pitchfork (PF) bifurcation at $\lambda = 0$ and a Hopf bifurcation at $\kappa = 0$ with $\lambda \geq 0$.

Periodic orbits will be described by symbol sequences of x's and y's, indicating how the orbit loops around the right ($v > 0$) or the left ($v < 0$) equilibrium points, following the notation of Sparrow [27]. The simplest orbits are the x- and y-orbits, created in a Hopf bifurcation from the nontrivial equilibrium points. These two orbits, which are related by the symmetry of the model, are jointly referred to as the x-orbits. Asymmetric orbits will be prefixed with an A unless there is an odd number of symbols in the sequence (in which case the orbit is bound to be asymmetric). Bifurcations will be prefixed with the simplest orbit involved in the bifurcation; for example, the Hopf bifurcation from the nontrivial equilibrium points, at which the x-orbits are created, is the x-Hopf bifurcation.

The point C ($\kappa = \lambda = 0$) is the Takens–Bogdanov bifurcation point; if κ and λ are assumed to be small, (2) can be reduced to the normal form (1) of the Takens–Bogdanov bifurcation with reflection symmetry by scaling $(v, w, t, \kappa, \lambda) \to (\epsilon v, \epsilon^2 w, t/\epsilon, \epsilon\kappa, \epsilon^2\lambda)$ and rewriting the $\dot{w}$ equation as $w = v^2 - \epsilon\dot{w} = v^2 - 2\epsilon v\dot{v} + \mathcal{O}(\epsilon^2)$. When this is substituted into the $\ddot{v}$ equation, (1) is recovered, with $M < 0$ and $N > 0$. The solutions of this equation are well-known [3, 4]; two bifurcation diagrams (see Figure 1) illustrate the behaviour of the system in this régime. In Figure 1(a), with $Q > Q_{\mathrm{C}}$ ($\kappa + \lambda > 0$), there is a subcritical Hopf bifurcation; beyond this point, all trajectories escape to infinity. In Figure 1(b), with $Q < Q_{\mathrm{C}}$ ($\kappa + \lambda < 0$), there is a supercritical pitchfork (PF) bifurcation, in which the non-trivial equilibrium points are created. These undergo a supercritical x-Hopf bifurcation, and a symmetric pair of x-orbits is created. As R increases further, these asymmetric orbits "glue" together to form a symmetric xy-orbit at a double homoclinic (x-gluing) bifurcation [28]; this new orbit is destroyed at an xy-saddle-node (xy-SN) bifurcation with the unstable orbit that was created in the subcritical Hopf bifurcation. Thus as we decrease Q below Q_{C}, the subcritical Hopf bifurcation from the trivial solution climbs up onto the steady branch and becomes a supercritical x-Hopf bifurcation.

We find numerically that for $\kappa > -0.25$, the large-amplitude behaviour of the ODEs is unstable, while for $\kappa < -0.25$, the global behaviour is stable. Thus for more negative values of κ and λ, the xy-orbit in Figure 1(b) is destroyed not in an xy-saddle-node bifurcation, but by becoming unbounded in amplitude, at a point we will call an xy-infinity bifurcation. This "bifurcation at infinity" requires us to distinguish carefully between the features of the model ODEs (2) that we would expect to find and those that we would not expect to find if we solved the PDEs for two-dimensional convection in a vertical magnetic field. Since the model was derived directly from the PDEs in the limit of narrow rolls using perturbative techniques [10, 11], any order-one bifurcation or periodic orbit found in the model will also occur in the PDEs, provided that the rolls are made narrow enough. Just how narrow the rolls must be depends on which feature we are looking for: bifurcations far from the point C will require narrower rolls than bifurcations near the point C. However, models derived by perturbative methods cannot capture global changes in stability; indeed, the dynamics of the PDEs for magnetoconvection must always be bounded, so the unbounded trajectories of (2) must be outside the range of validity of the model. This problem is removed by including the $\mathcal{O}(\varpi)$ terms in (2) and examining the corrected model [11]:

$$\begin{aligned} \ddot{v} &= \kappa\dot{v} - \lambda v - vw + \frac{\varpi}{4-\varpi}(A_1 v + A_2\dot{v} + A_3 vw + A_4\dot{v}w + A_5 v^3) + \mathcal{O}(\varpi^2), \\ \dot{w} &= -w + v^2 - \frac{\varpi}{4-\varpi}(v^2 + 4v\dot{v}) + \mathcal{O}(\varpi^2), \end{aligned} \tag{3}$$

where $A_1, \ldots, A_5$ are constants that depend on σ, ζ (the Prandtl numbers) and κ and λ:

$$\begin{aligned} A_1 &= -2\lambda\left(1 - \frac{2\kappa}{1+\sigma+\zeta}\right), \qquad A_2 = \kappa\left(1 - \frac{4\kappa}{1+\sigma+\zeta}\right), \\ A_3 &= -4\kappa\frac{1+\sigma+\zeta+(\sigma+\zeta)^2}{(1+\sigma+\zeta)(\sigma+\zeta)} - 2\frac{\zeta+\sigma\zeta+\zeta^2-2\sigma-2}{\zeta(1+\sigma+\zeta)}, \\ A_4 &= -4\frac{1+\sigma}{\zeta(1+\sigma+\zeta)}, \qquad A_5 = -2\frac{(1+3\sigma+3\zeta)(1+\sigma)}{\zeta(1+\sigma+\zeta)(\sigma+\zeta)}. \end{aligned}$$

Clearly, the corrected model (3) reduces to (2) when $\varpi \to 0$, and any bounded solution of (2) will be reproduced (with $\mathcal{O}(\varpi)$ corrections) in (3) if ϖ is small enough. It is found numerically that in the corrected model, trajectories do not escape to infinity for order-one values of κ and λ of either sign. For example, at the point C, trajectories of (3) are attracted to a large ($\mathcal{O}(\varpi^{-1})$) stable periodic orbit; the same occurs in the PDEs [11].

The inclusion of $\mathcal{O}(\varpi)$ corrections, while desirable from the point of view of eliminating the unrealistic xy-infinity bifurcation seen in (2), makes the analysis of the ODEs much more involved. Therefore in this paper we restrict our attention to (2), with the understanding that the only trajectories that are relevant to magnetoconvection are those that are bounded. If ϖ is small enough, then the only effect that the $\mathcal{O}(\varpi)$ corrections in (3) will have for order-one values of κ and λ is to eliminate the xy-infinity bifurcation.

The precise unfolding diagram with the $\mathcal{O}(\varpi)$ corrections included is left for another paper [11], but an analogy with the results of [29, 30] suggests what will occur near the bifurcation point C. The second-order amplitude equation (1) with $M < 0$ and $N > 0$ has the bifurcations depicted in Figure 1, with trajectories that escape to infinity if R is larger than a certain value. Indeed, this equation is known to have "bifurcations at infinity" for other values of M and N [6]. Addition of appropriate quintic terms, which play the same role as the $\mathcal{O}(\varpi)$ corrections in (3), make the global behaviour stable [29]. For example, in this problem with $M < 0$ and $N > 0$, it is easy to see that adding $-a^4\dot{a}$ to the right-hand side of (1) achieves this result. In this case, the unstable periodic orbits created in the subcritical Hopf bifurcation at $\kappa = 0$ turn around in an xy-saddle-node bifurcation (instead of going to infinity) and become large-amplitude stable periodic orbits. This new line of xy-saddle-node bifurcations connects to the line of xy-saddle-node bifurcations that emerges from the point C in a cusp [29, 30]. Thus we expect that the xy-infinity bifurcation in (2)

will be replaced by an xy-saddle-node bifurcation when the $\mathcal{O}(\varpi)$ corrections are included, and that trajectories that would have escaped to infinity will instead be attracted to large-amplitude stable periodic orbits.

3. Homoclinic explosions

The nature of the homoclinic bifurcation depends on the dominant eigenvalues (those eigenvalues, positive or negative, that are closest to zero) of the trivial solution and on the geometry of the homoclinic trajectories. Near the point C in the (κ, λ) plane (see Figure 2), the orbits involved in the x-gluing bifurcation are in the figure-of-eight configuration [28]: the homoclinic trajectories approach and leave the trivial solution in the $(v, \dot{v})$ plane. At the point A ($(\kappa, \lambda) \approx (-0.501, -0.499)$) where the two negative eigenvalues of the trivial solution are equal, the homoclinic trajectories switch to the butterfly configuration: they approach the trivial solution downwards along the w-axis and leave it in the $(v, \dot{v})$-plane. Between points A and B ($(\kappa, \lambda) \approx (-1.724323, -2.724323)$), the negative eigenvalue corresponding to the w-axis is larger in magnitude than the positive eigenvalue in the $(v, \dot{v})$ plane, so orbits approaching the homoclinic (gluing) bifurcation must be stable [4]. At the point B, the two eigenvalues closest to zero are equal in magnitude; beyond B, the positive eigenvalue is larger in magnitude than the negative one, so the orbits approaching the homoclinic bifurcation must be unstable. The homoclinic bifurcation can no longer be a gluing bifurcation. We will see below that the x-gluing bifurcation splits into many bifurcations; the four principal ones are: an x-homoclinic explosion, an x-saddle-node bifurcation, a subcritical xy-symmetry-breaking bifurcation and an Axy-homoclinic explosion. Chaotic trajectories are found in between the two homoclinic explosions.

The transition at the point B can be understood in terms of a one-dimensional map that models the flow there [24, 31, 32]. This map is constructed in the standard fashion [33]. First, the ODEs (2) are diagonalised:

$$\begin{aligned} \dot{x} &= s_p x - (x+y)z/(s_p - s_m), \\ \dot{y} &= s_m y + (x+y)z/(s_p - s_m), \\ \dot{z} &= -z + (x+y)^2, \end{aligned} \tag{4}$$

where x and y are linear combinations of v and $\dot{v}$, $z = w$, and s_p, s_m and -1 are the three eigenvalues of (2), with $s_p > 0$ and $s_m < -1$.

Next, a two-dimensional return map near the homoclinic trajectory is constructed (see Figure 3). Near the homoclinic bifurcation, trajectories that start in a neighbourhood of the trivial solution will leave along the x-axis (the unstable manifold) and return to the neighbourhood downwards near the z-axis. If we construct a small box around the trivial solution in which the flow is nearly linear, the map defined by the flow inside the box from the top of the box ($z = h$) to the sides can be calculated explicitly. Outside the box, the flow is given approximately by an affine map from the sides of the box back to the top. The approximations made in constructing this map are good as long as the box is small enough and the homoclinic trajectory does not go near any other equilibrium point. Composing the two maps yields a two-dimensional map from the plane $z = h$ back to itself. Finally, the two-dimensional map reduces to a one-dimensional Lorenz map f as there is strong contraction in the y direction:

$$f : x \to \mathrm{sign}(x) \left(-\mu + a \left| x \right|^{\delta} \right). \tag{5}$$

The parameter δ is the saddle index, the ratio of the dominant eigenvalues: $\delta = |-1/s_p|$; $\delta > 1$ between points A and B, and $\delta < 1$ beyond point B. The parameter a depends on the global properties of the flow; the parameter μ gives the x-coordinate at which the unstable manifold of the origin returns to the plane $z = h$. Fixed points of the map correspond to x-orbits; fixed points of the second iterate of the map correspond to xy- or Axy-orbits, and so on. Homoclinic orbits occur when 0 is mapped back onto itself, so the x-homoclinic bifurcation occurs when $f(0^{\pm}) = 0$, or $\mu = 0$.

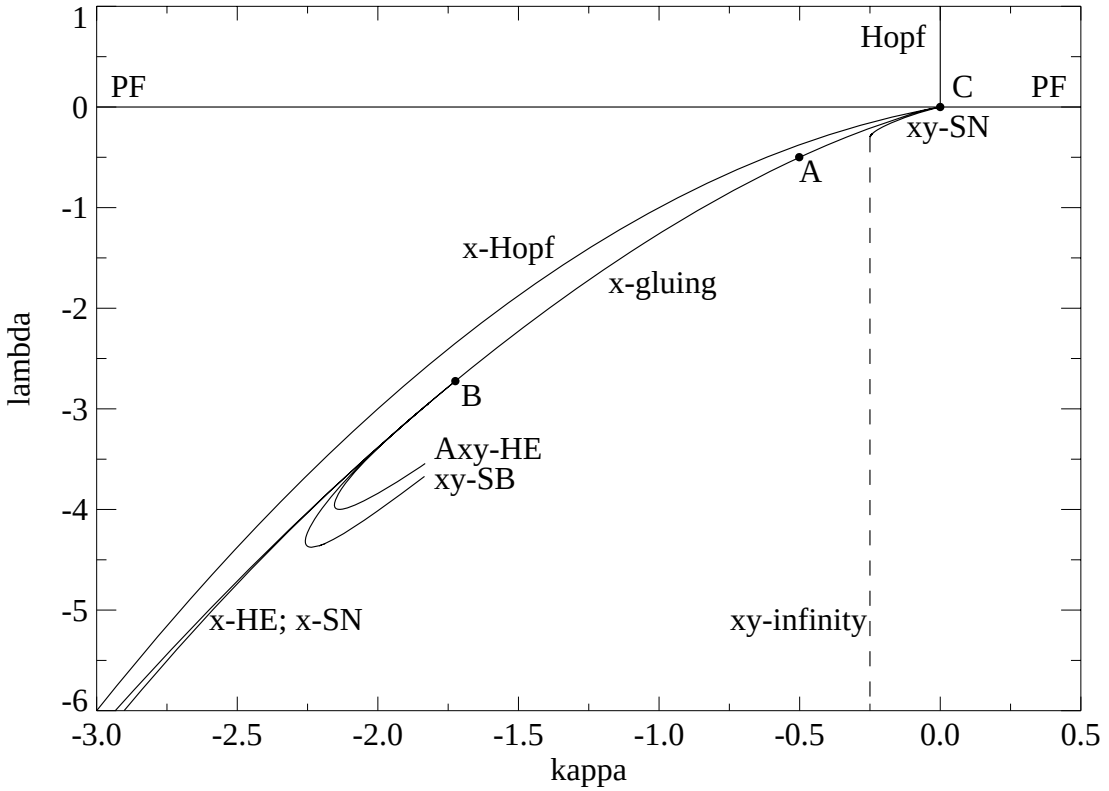

Figure 2. *Numerically computed unfolding diagram near the points C and B. Near the point C, there are two bifurcations from the trivial solution: the Hopf bifurcation and the pitchfork (PF) bifurcation. The three bifurcation lines emerging from the point C towards negative κ and λ are (from top to bottom), the x-Hopf, the x-gluing and the xy-saddle-node (xy-SN) bifurcations. The vertical dashed line on the right (xy-infinity) indicates where the xy-orbits become unbounded; to the right of this line (2) has no attracting set. At point A, the homoclinic trajectories involved in the x-gluing bifurcation switch from the figure-of-eight configuration to the butterfly configuration. The x-gluing bifurcation splits at the point B into four bifurcations: an x-homoclinic explosion (x-HE), an x-saddle-node (x-SN) bifurcation, a subcritical xy-symmetry-breaking (xy-SB) bifurcation and an Axy-homoclinic explosion (Axy-HE). The wedge below the point B that contains the chaotic trajectories (between the x-HE (leftmost) and Axy-HE (rightmost) lines) is narrow at first, but broadens as λ decreases. There are three bifurcation lines leaving the figure at the bottom left corner; these are (from top to bottom) the x-Hopf, the x-HE and the x-SN bifurcation lines.*

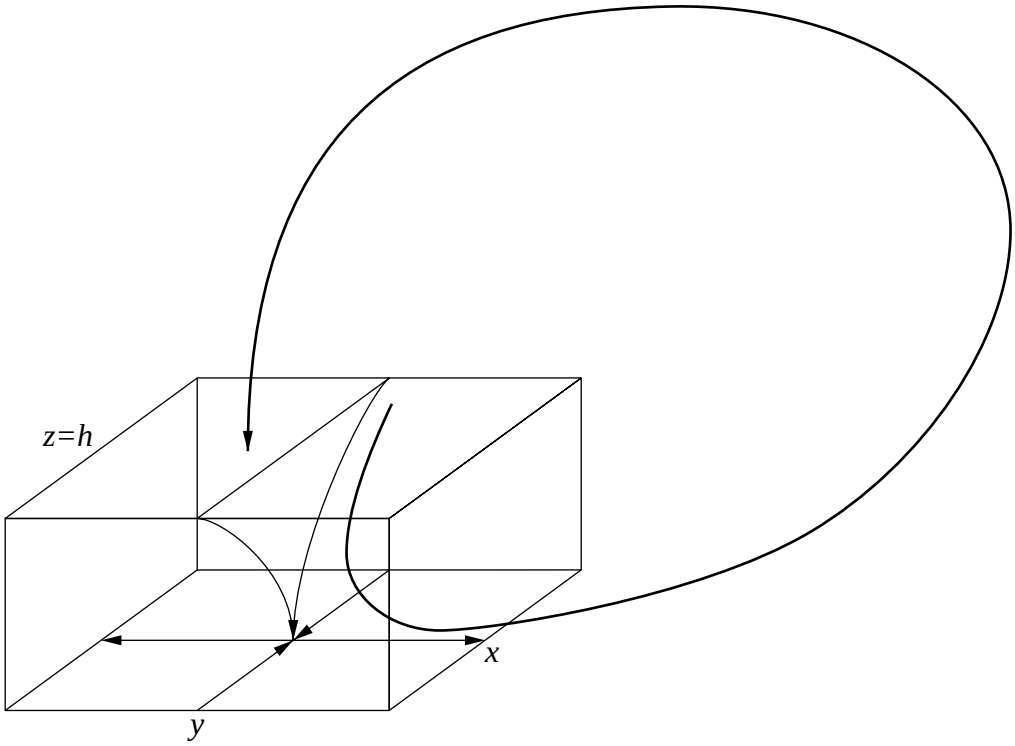

Figure 3. *The Poincaré map. A trajectory starting at a point on $z = h$ goes through the box, out along the unstable manifold of the origin (tangent to the x-axis), and returns to $z = h$.*

The analysis of the map [24, 34, 31] will be illustrated by considering the value of μ at which the image of 0 under the second iterate of the map is 0 – this corresponds to an Axy-homoclinic bifurcation. This value $\mu = \mu_*$ will satisfy $f^2(0^{\pm}) = 0$, which yields

$$\mu_* = \mathrm{sign}(a)\,|a|^{1/(1-\delta)}\,. \tag{6}$$

If μ_* is viewed as a function of δ, there is a singularity in the relationship at the point B, where $\delta = 1$. If $|a| < 1$, the line $\mu_*(\delta)$ goes to infinity as δ tends to 1^+, and $\mu_*(\delta)$ goes to zero as δ tends to 1^-; the opposite occurs if $|a| > 1$. Thus the line $\mu_*(\delta)$ will connect to the point B on only one side; which side it is depends only on the value of $|a|$ compared to 1.

Numerical estimates of a (discussed below) yield $0 < a < 1$ near the point B, which implies that the Axy-homoclinic bifurcation line exists below B, where $\delta < 1$. Thus the line $\mu = 0$ is an x-gluing bifurcation for $\delta > 1$, and splits into an x-homoclinic bifurcation ($\mu = 0$) and an Axy-homoclinic bifurcation ($\mu = \mu_*$) below the point B. In fact, these two homoclinic bifurcations are homoclinic explosions [27], in which an infinite number of unstable periodic and aperiodic trajectories are created or destroyed. The strange invariant set created in the homoclinic explosion becomes an attractor for a range of values of μ in between 0 and μ_*. There is thus a band of chaotic trajectories in between the two homoclinic explosions – a schematic bifurcation diagram is shown in Figure 4. The unstable periodic and aperiodic trajectories created in the x-homoclinic explosion (x-HE) are all destroyed by the time we reach the Axy-homoclinic implosion (Axy-HE), with the exception of the xy-orbit, which has gained stability in a subcritical xy-symmetry-breaking (xy-SB) bifurcation and emerges at the right of the figure. The unstable Axy-orbit created in the xy-symmetry-breaking

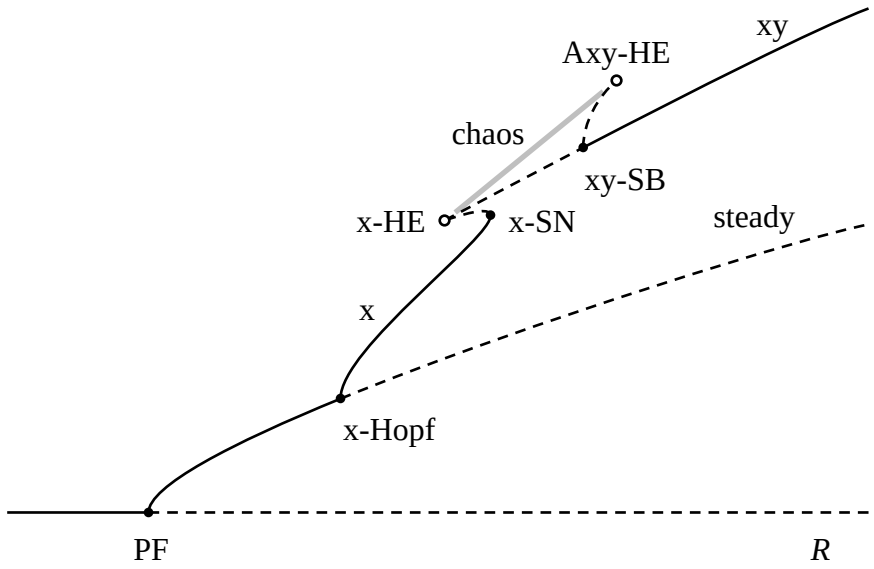

Figure 4. *Schematic bifurcation diagram just beyond the point B ($\delta < 1$), showing how the x-gluing bifurcation (see Figure 1(b)) has split into a homoclinic explosion/implosion pair, with an interval of stable chaos in between.*

bifurcation is destroyed in the Axy-homoclinic implosion. The unstable x-orbit created in the x-homoclinic explosion is destroyed in an x-saddle-node (x-SN) bifurcation with the stable x-orbit created in the x-Hopf bifurcation. In between the x- and Axy-homoclinic explosions is an interval of stable chaos.

The map (5) is a good model of the flow when x and μ are small. As B is approached from below ($\delta < 1$), the map has attracting chaotic trajectories for arbitrarily small values of x and μ; thus near the point B, the model ODEs have chaotic trajectories created in a homoclinic explosion, in the same manner as the chaotic trajectories of the Lorenz equations [27].

A comparison of the map and ODE brute force bifurcation diagrams is made in Figure 5, which shows that the ODEs near the point B are described strikingly well by the one-dimensional map. In this figure, we see the x-orbit entering on the left, the xy-orbit leaving on the right, and the interval of chaos in between. Note that this chaotic régime is very simple, in that there are no periodic windows.

The map parameter a may be estimated numerically by recording successive intersections of a trajectory with a particular plane $z = h$, and fitting these data to a map of the form (5). When calculated in this fashion, a generally depends on h, but it can be shown that a does not depend on h at the point B, the only point at which the magnitude of a matters. At this point, we find $a \approx 0.62635$, which is less than the critical value $a = 1$.

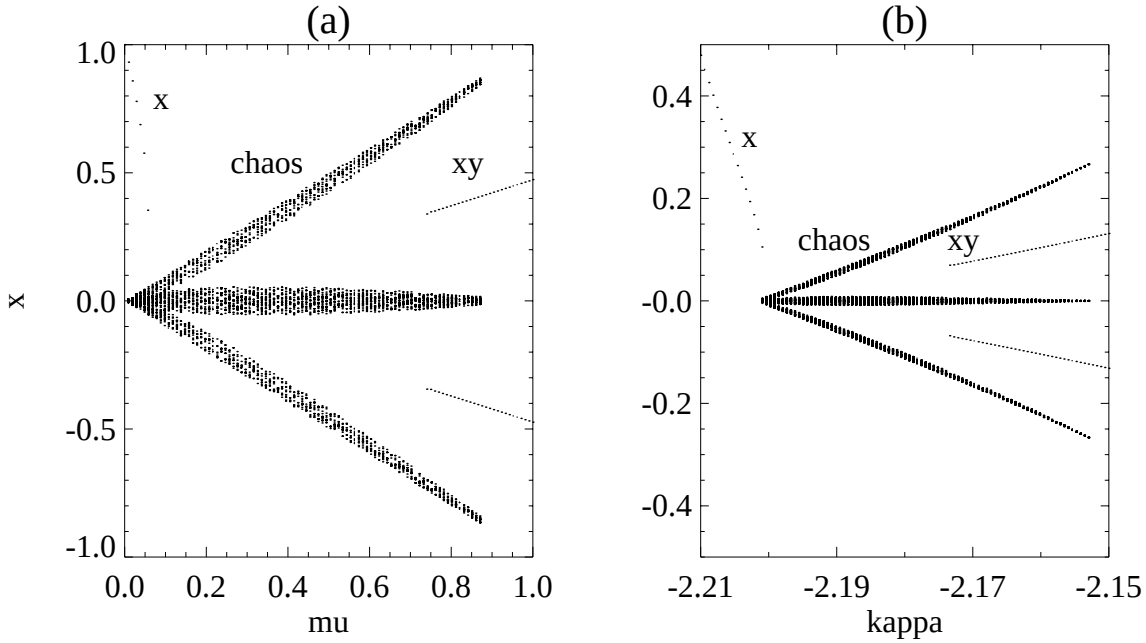

Figure 5. *Brute force bifurcation diagrams near the point B. (a) Bifurcation diagram for the map (5), with $\delta = 0.8579$ and $a = 1$. (b) Bifurcation diagram for (2), with $\lambda = -3.9$, just below the point B; the points that are plotted on the vertical axis are the x-coordinates of the intersection of the trajectory with the Poincaré return plane $z = 0.6$. The stable x- and xy-orbits and the stable chaotic trajectories are indicated.*

4. Creation of period-doubling bifurcations

The data presented in Figure 6 suggest that at some point, the map parameter a is zero at the homoclinicity. Define the codimension-two bifurcation point D to be that point at which there is an Axy-homoclinic bifurcation with $a = 0$. This is a new type of codimension-two bifurcation point. To analyse the transitions at D, we retain the next higher order term in the map, and obtain the map g:

$$g : x \to \mathrm{sign}(x) \left(-\mu + a\,|x|^{\delta} + b\,|x|^{2\delta} \right), \tag{7}$$

where μ and a are both zero at the point D, δ is less than one (but greater than $1/2$) and b is positive. We use the fact that $2\delta < |s_m/s_p|$ at the point D. Near D, we will see that the principal homoclinic orbit is an Axy-orbit (instead of an x-orbit near B), so fixed points of the map are Axy-orbits, fixed points of the second iterate are xyyx-, Axyyx- or Axyxy-orbits, and so on.

The map (7) cannot be justified as a good model of the flow in the same way that the map (5) could near the point B, because of the non-existence of a strong stable foliation when a is negative. Nonetheless, the map (7) is still a useful and remarkably good model of the flow.

The form of the map (7) as a decreases through zero is illustrated in Figure 7(a)–(c). Since the slope of the map can be negative when a is negative, it is possible to obtain period-doubling bifurcations. Moreover, with both μ and a negative, it is possible to get a disjoint pair of unimodal maps (Figure 7(d)), so we should expect to see the period-doubling cascades and periodic windows characteristic of the logistic map. Coste and Peyraud [35] have studied maps similar to those shown in Figure 7(c)–(d); they did not consider the possibility that a could go through zero.

We begin the analysis of the map (7) by considering the special case with $a = 0$: since b is positive and $2\delta > 1$, as μ increases through zero, a pair of stable Axy-orbits glue together to form a stable xyyx orbit. If a is positive (Figure 8(a)), we will have the same bifurcation diagram as in Figure 4, except that here the Axy-orbit plays the role of the x-orbit. The Axy-orbit turns around

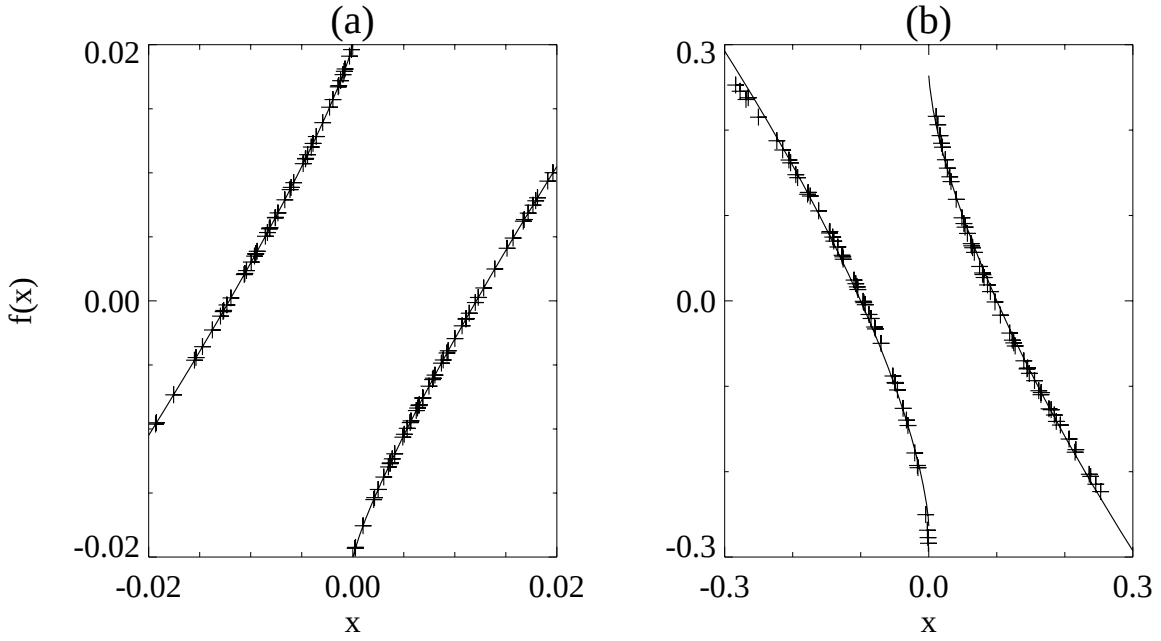

Figure 6. *Numerically computed Poincaré maps near the point D. (a)* $(\kappa, \lambda) = (-1.07, -2.7)$ *with a return plane at* $z = 0.05$. *(b)* $(\kappa, \lambda) = (-1.18, -3.9)$ *with a return plane at* $z = 0.4$. *The crosses are computed by integrating the ODEs (2) and recording the* x*-coordinate of the intersection of the trajectory with the return plane; each value of* x *is plotted against the value of* x *for the previous intersection. The data are fitted to maps (shown as solid lines) of the form in equation (5); the fitting parameters are: (a)* $\delta = 0.83817$, $\mu = 0.0200487$ *and* $a = 0.81092$*; (b)* $\delta = 0.67976$, $\mu = -0.264$ *and* $a = -1.261$.

in an Axy-saddle-node bifurcation and is destroyed in an Axy-homoclinic explosion. The xyyx-orbit created in this explosion is stabilised by a subcritical xyyx-symmetry-breaking bifurcation, and there is an interval of stable chaos between the Axy- and the Axyyx-homoclinic explosions. The situation with a negative is similar (Figure 8(b)), but instead of a symmetry-breaking bifurcation from the xyyx-orbit, there is a subcritical period-doubling bifurcation from the Axy-orbit, creating an unstable Axyxy-orbit that is destroyed in the Axyxy-homoclinic explosion. Again there is an interval of stable chaos, this time between the Axy- and Axyxy-homoclinic explosions.

The value μ_* that we used near the point B is here viewed as a function of a: at the point D, $a = 0$ and $\mu_*(0) = 0$, so the lines of Axyyx-homoclinic explosions ($a > 0$) and of Axyxy-homoclinic explosions ($a < 0$) must both connect to the point D, but on opposite sides of the line of Axy-homoclinic explosions. These results are summarised in a schematic unfolding diagram of the point D in Figure 9: we see that a homoclinic explosion (Axy-HE) can change the direction in which the strange invariant set is produced if the global parameter a goes through zero.

A comparison of the map and ODE bifurcation diagrams for $a < 0$ is made in Figure 10. In both diagrams, we see the Axy-orbit entering on the right and the xyyx-orbit leaving on the left, with an interval of chaos in between. As in the case with $a > 0$ (Figure 5), the map bifurcation diagram agrees strikingly well with the ODE bifurcation diagram.

The numerically computed unfolding diagram (see Figure 11) shows how the point D fits in. The Axy-homoclinic explosion and xy-symmetry-breaking bifurcation lines start at B then loop back towards smaller values of λ, before turning again and heading for more negative values of λ. The xy-symmetry-breaking bifurcation becomes supercritical at the point E ($(\kappa, \lambda) \approx (-1.192, -2.497)$) when it emits an Axy-saddle-node bifurcation line. This line connects to the Axy-homoclinic explosion line at the point D ($(\kappa, \lambda) \approx (-1.087, -3.096)$), where the line of subcritical Axy-period-doubling

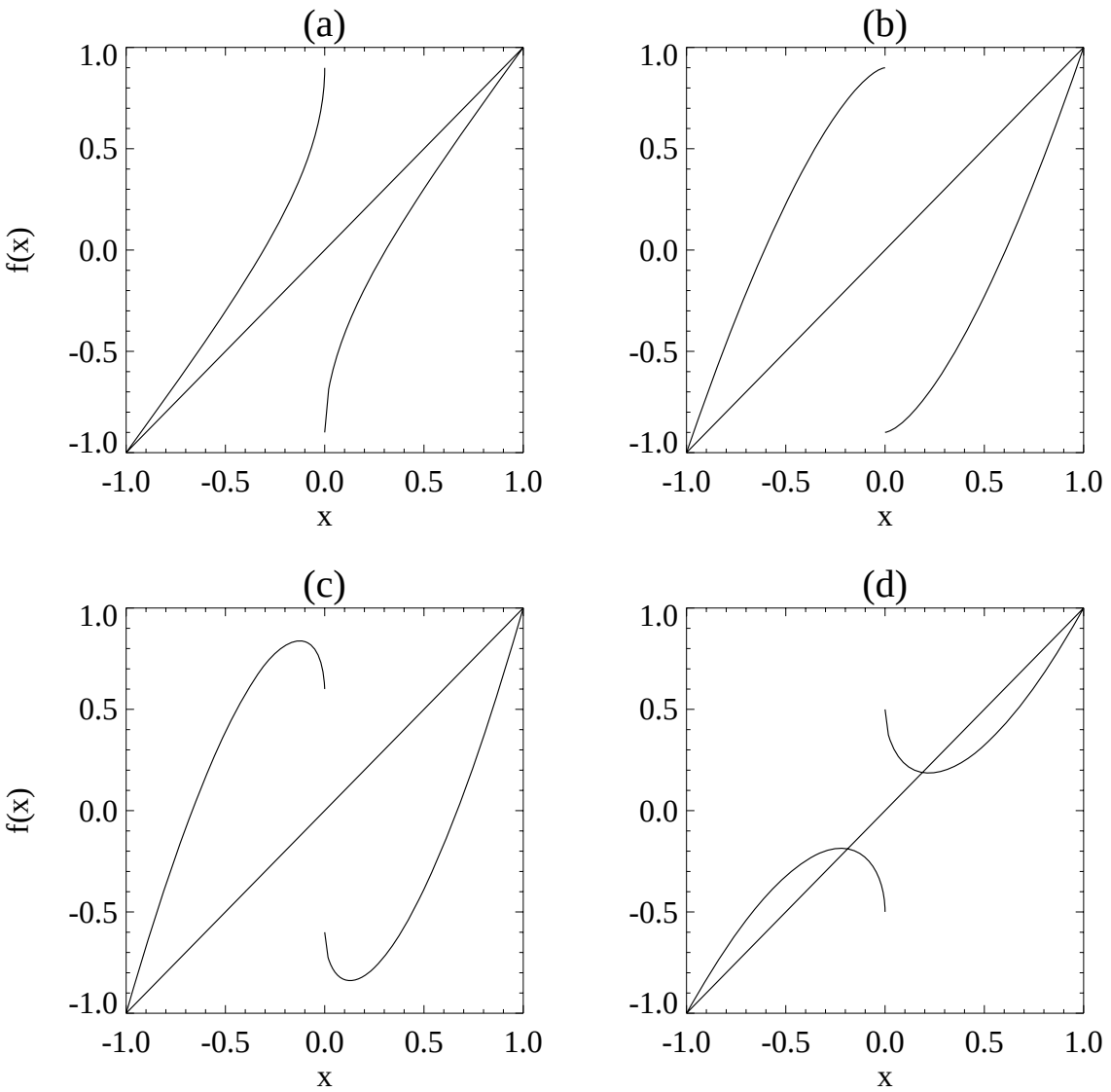

Figure 7. *The one-dimensional map (7), with $b > 0$ and $1/2 < \delta < 1$. (a) $a > 0$, (b) $a = 0$, (c) $a < 0$, all with $\mu > 0$. (d) $a < 0$ with $\mu < 0$.*

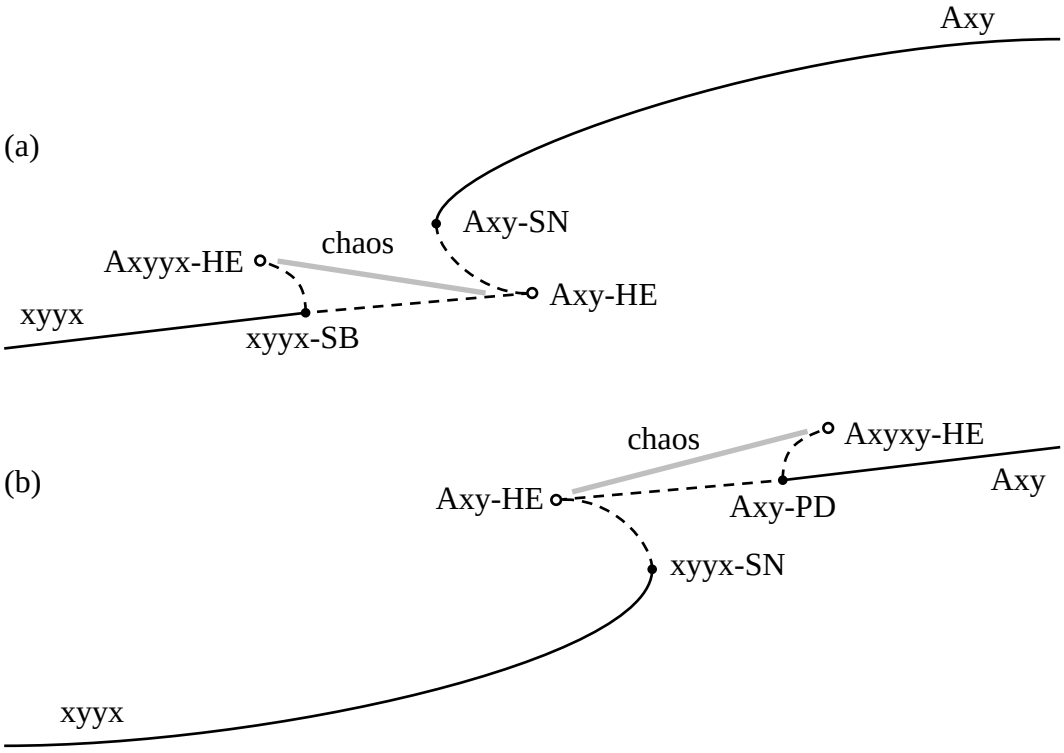

Figure 8. *Schematic bifurcation diagrams for the map (7) near the point D, showing the two ways of going from Axy-orbits to xyyx-orbits. (a) $a > 0$; (b) $a < 0$. As in the other schematic bifurcation diagrams, the Rayleigh number increases to the right, although μ increases to the left.*

(Axy-PD) bifurcations is created.

The entire unfolding diagram for the parameter range we have studied so far is shown schematically in Figure 12. This global picture also shows the principal attracting sets for the various parameter régimes: there are large regions of attracting chaotic trajectories, as well as regions where x-, xy-, Axy- and xyyx-orbits are stable.

As we continue to more negative λ, the Axy-period-doubling bifurcation becomes supercritical by emitting an Axyxy-saddle-node bifurcation, which then combines with the Axyxy-homoclinic explosion created at D to produce a subcritical Axyxy-period-doubling bifurcation at a codimension-two point of the same type as the point D. The subcritical Axyxy-period-doubling bifurcation in turn becomes supercritical by creating another saddle-node bifurcation, which then combines with a homoclinic explosion at yet another codimension-two bifurcation point, to produce the next higher subcritical period-doubling bifurcation. This process of the creation of period-doubling bifurcations continues, and accumulates in what appears to be an infinite cascade of supercritical period-doubling bifurcations by $\lambda \approx -6$, beyond which point we would expect the familiar scenario of chaos interspersed with periodic windows and period-doubling cascades. The existence of a period-doubling cascade suggests that there may be Shil'nikov bifurcations nearby; we show in the next section that this is the case.

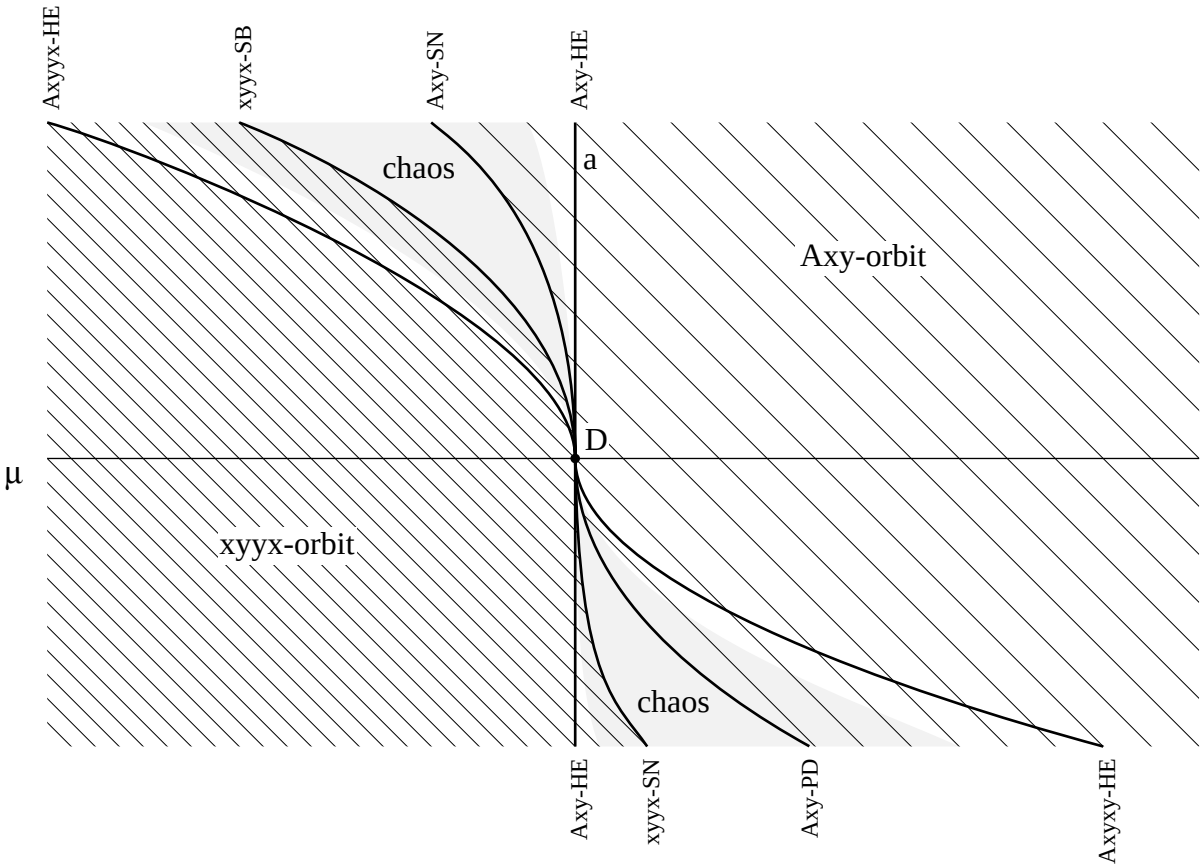

Figure 9. *Schematic unfolding diagram for the map (7) near the point D. We have the Axy- and Axyyx-homoclinic explosions entering the point D from above ($a > 0$), and the Axy- and Axyxy-homoclinic explosions leaving from below ($a < 0$). In these two wedges above and below the point D, there are regions (shaded) with attracting chaotic trajectories. The single and double hatching indicates the region of stability of the Axy- and xyyx-orbits respectively.*

5. The T-point

When the parameter a is positive, the map (5) is orientation-preserving, that is, the homoclinic trajectory undergoes an even number of half-twists before returning to the origin, and when a is negative, the map is orientation-reversing, and the homoclinic trajectory undergoes an odd number of half-twists. Thus when a goes through zero, the homoclinic trajectory must have increased (or decreased) its twist by one half turn. The Axy-homoclinic explosion that emerges from the point B does this once, at the point D. There are, however, other homoclinic bifurcations that do this repeatedly: the parameter a crosses from positive to negative and back, each time accumulating a twist on the homoclinic trajectory. Such a sequence of orbits is illustrated in Figure 13(a)–(c). It is clear that the homoclinic trajectory is twisting as it approaches the unstable nontrivial equilibrium point, which is a saddle-focus. At the point T ($(\kappa, \lambda) \approx (-2.0, -6.6)$), there is a double heteroclinic connection between the trivial solution and the two unstable equilibrium points (see Figure 13(c); for clarity, only one of the two connections is shown). If we allow AUTO to continue to follow the orbits with large period, we find that the homoclinic orbits, having established a heteroclinic connection with a nontrivial equilibrium point, now disconnect from the trivial solution and we are left with a homoclinic connection to a saddle-focus (Figure 13(d)).

The lines of homoclinic bifurcations leading to the point T are shown in Figure 14. The numerically computed unfolding diagram about the point T agrees with the known results [36, 37]. Emerging from the point T are a logarithmic spiral of homoclinic bifurcations involving the trivial

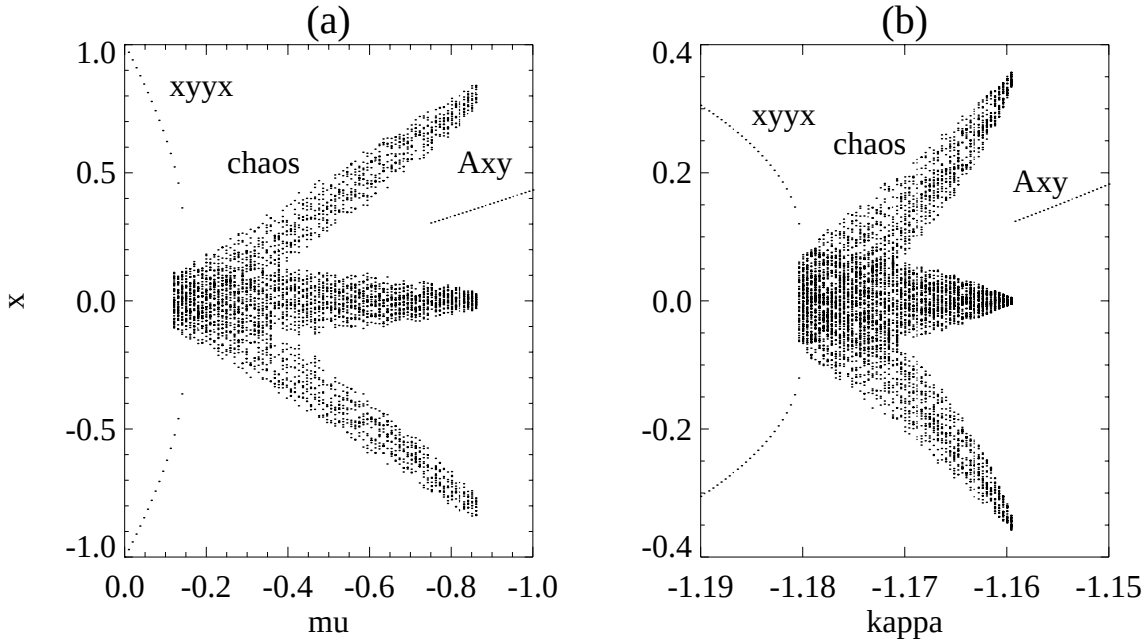

Figure 10. *Brute force bifurcation diagrams with $a < 0$, near the point D. (a) Bifurcation diagram for the map (7), with $\delta = 0.6781$, $a = -1$ and $b = 0$. (b) Bifurcation diagram for (2), with $\lambda = -3.9$; the points that are plotted on the vertical axis are the x-coordinates of the intersection of the trajectory with the Poincaré return plane $z = 1.0$.*

solution and a straight line of homoclinic connections to the non-trivial equilibrium points. These equilibrium points are saddle-foci and satisfy Shil'nikov's [14] condition; we therefore expect to see chaos associated with period-doubling cascades and orbits "wiggling" their way towards homoclinicity [38, 39] in between the two lines labelled SN on the figure, which limit the first two Shil'nikov wiggles.

Each time that the logarithmic spiral winds towards the point T, the homoclinic trajectory has accumulated one more full twist, so the one-dimensional map parameter a must have changed sign twice. This suggests that there is a codimension-one line $a = 0$ that crosses the logarithmic spiral and passes through the points D and T [23]. The lines of saddle-node bifurcations (labelled SN in Figure 14) that limit the first two of the Shil'nikov wiggles connect to the logarithmic spiral presumably at points where $a = 0$, so it will be possible to analyse these codimension-two points; the analysis is not attempted in this paper. In between the two lines of saddle-node bifurcations are the period-doubling cascades and inverse cascades associated with the Shil'nikov bifurcation.

The Axyyx-homoclinic explosion line, which emerges from the point D, winds up in another logarithmic spiral around the point T_2. This shows that there is a connection between T-points (codimension-two points of the type T and T_2) with their period-doubling cascades on the one hand, and the creation of period-doubling bifurcations as described in the previous section on the other. In the first situation, chaotic trajectories are seen as the accumulation of an infinite number of supercritical period-doubling bifurcations, whereas in the second, chaotic trajectories are created abruptly in a homoclinic explosion associated with a subcritical period-doubling bifurcation. Understanding how these two are related would involve a more complete analysis of the one-dimensional map (7) and the two-dimensional map that describes the flow near the point T [37].

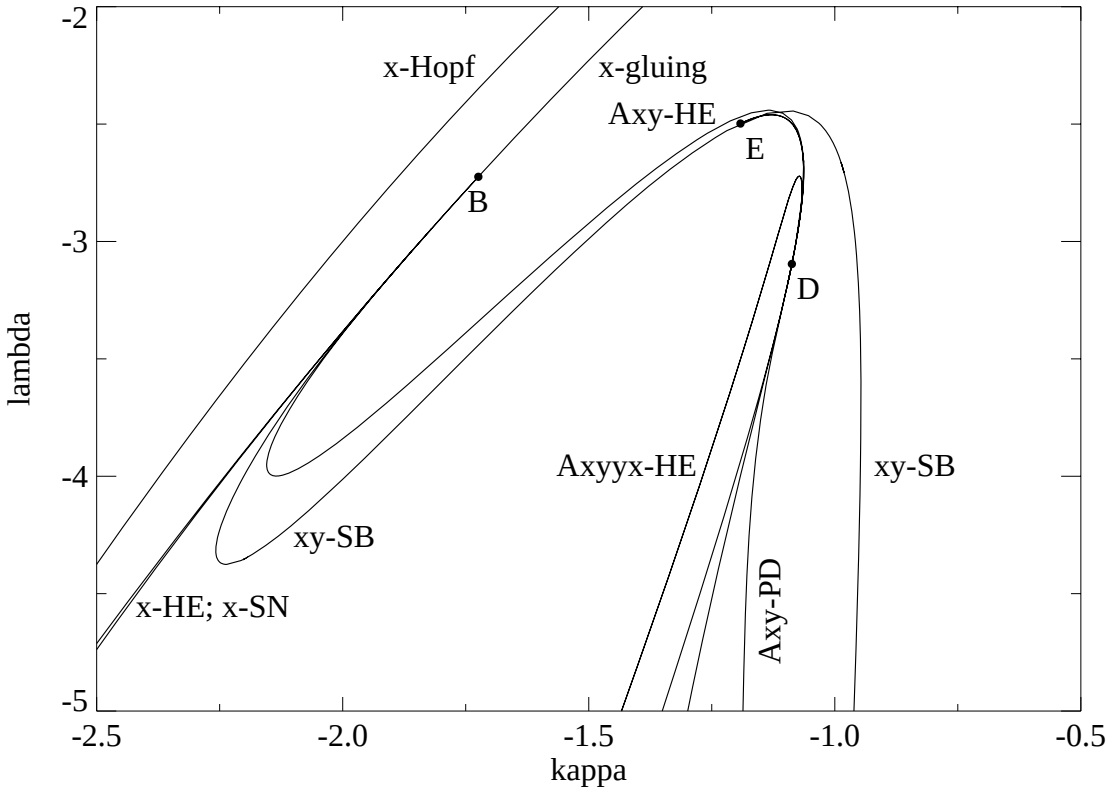

Figure 11. *Numerically computed unfolding diagram for $-2 \geq \lambda \geq -5$, showing the bifurcations involving the simplest orbits. The x-homoclinic explosion and x-saddle-node bifurcation lines that start at B continue towards more negative values of κ and λ. Three bifurcation lines are shown below the point D, which are (from left to right) the Axy-HE, the xyyx-SN (both unlabelled) and Axy-PD bifurcation lines. The Axy-SN bifurcation line connecting the points D and E is also unlabelled.*

6. Concluding remarks

The complete analysis of a chaotic set of ODEs like (2) is of course impossible; the best we can hope for is a description of the bifurcations of the simplest orbits and an understanding of how the chaotic trajectories arise. In this system, there are several codimension-two homoclinic bifurcation points (C, B and D) near which we can analyse the flow in some detail. The unfolding of the Takens–Bogdanov bifurcation point C is well-known [3, 4]. Near B and D, the unfolding diagram is found by constructing one-dimensional maps. The first homoclinic explosions and chaotic trajectories are created at the point B [24, 31]. The new bifurcation point D, at which a subcritical period-doubling bifurcation is created, presents the possibility of understanding how chaotic trajectories created in a homoclinic explosion relate to chaotic trajectories created in a period-doubling cascade. At the codimension-two heteroclinic bifurcation point T [36, 37], we see the creation of a line of Shil'nikov bifurcations, with the associated period-doubling cascades, wiggles and chaotic trajectories.

Equations (2) provide an asymptotically exact description of the PDEs that govern two-dimensional convection in an imposed vertical magnetic field, in the limit of narrow rolls [10, 11]. This implies that the bifurcation structure and the chaos of the ODEs will appear in the PDEs. This is a significant result, as it is often difficult to understand the origins of chaos in sets of nonlinear PDEs. Chaos associated with period-doubling cascades and Shil'nikov bifurcations has been observed in the PDEs governing thermosolutal convection [40], and is related to chaos and period-doubling cascades found in the asymptotically exact model of this problem [12]. Numerical

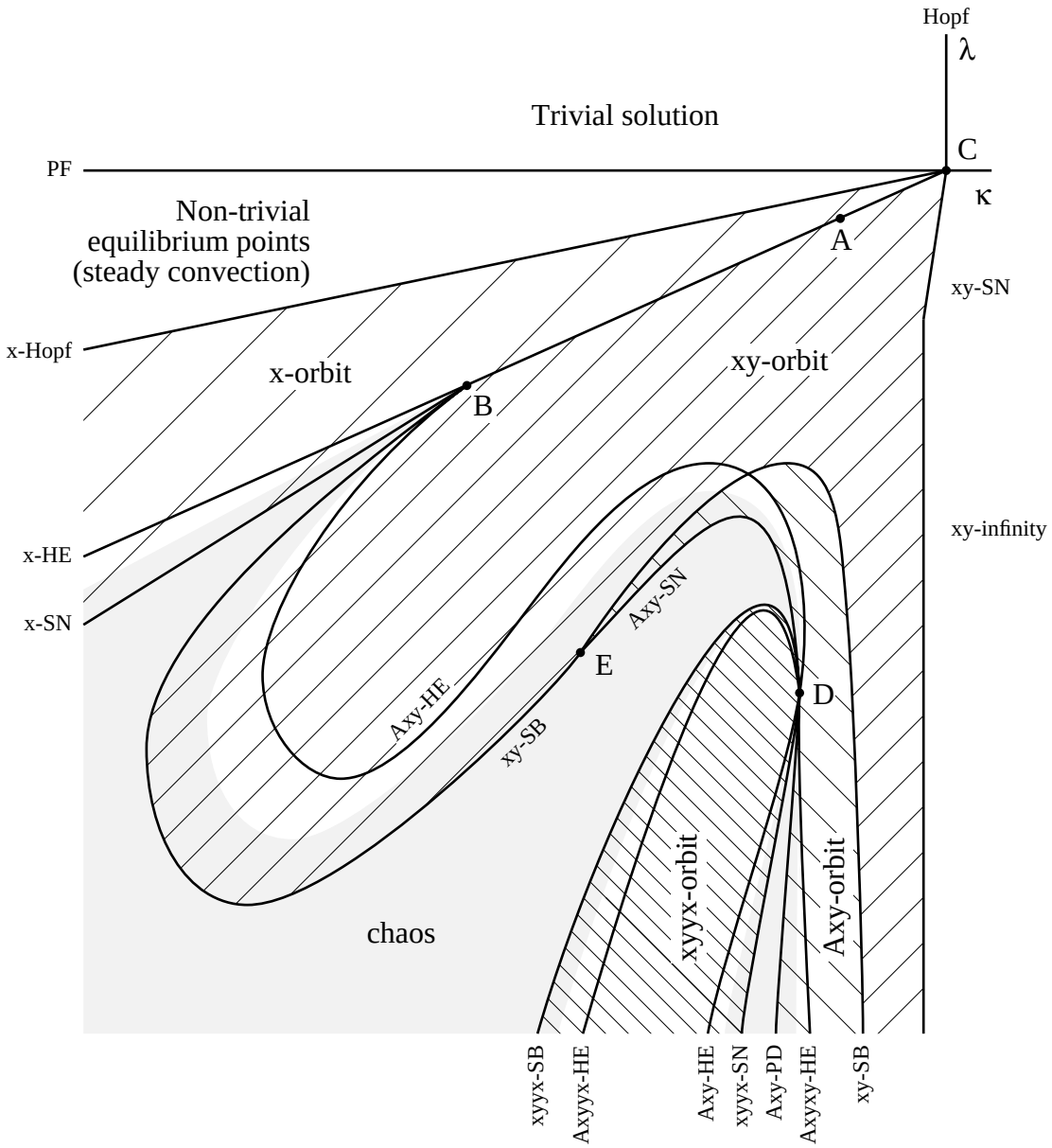

Figure 12. *Schematic unfolding diagram, showing the principal bifurcations and attracting sets of (2) as a function of κ and λ. The domains of stability of the four simplest periodic orbits are shown as hatched regions: the x- and xy-orbits are singly and doubly hatched, slanting upwards to the right, and the Axy- and xyxy-orbits are doubly and quadruply hatched, slanting downwards to the right. The regions with attracting chaotic trajectories are shown as tinted grey.*

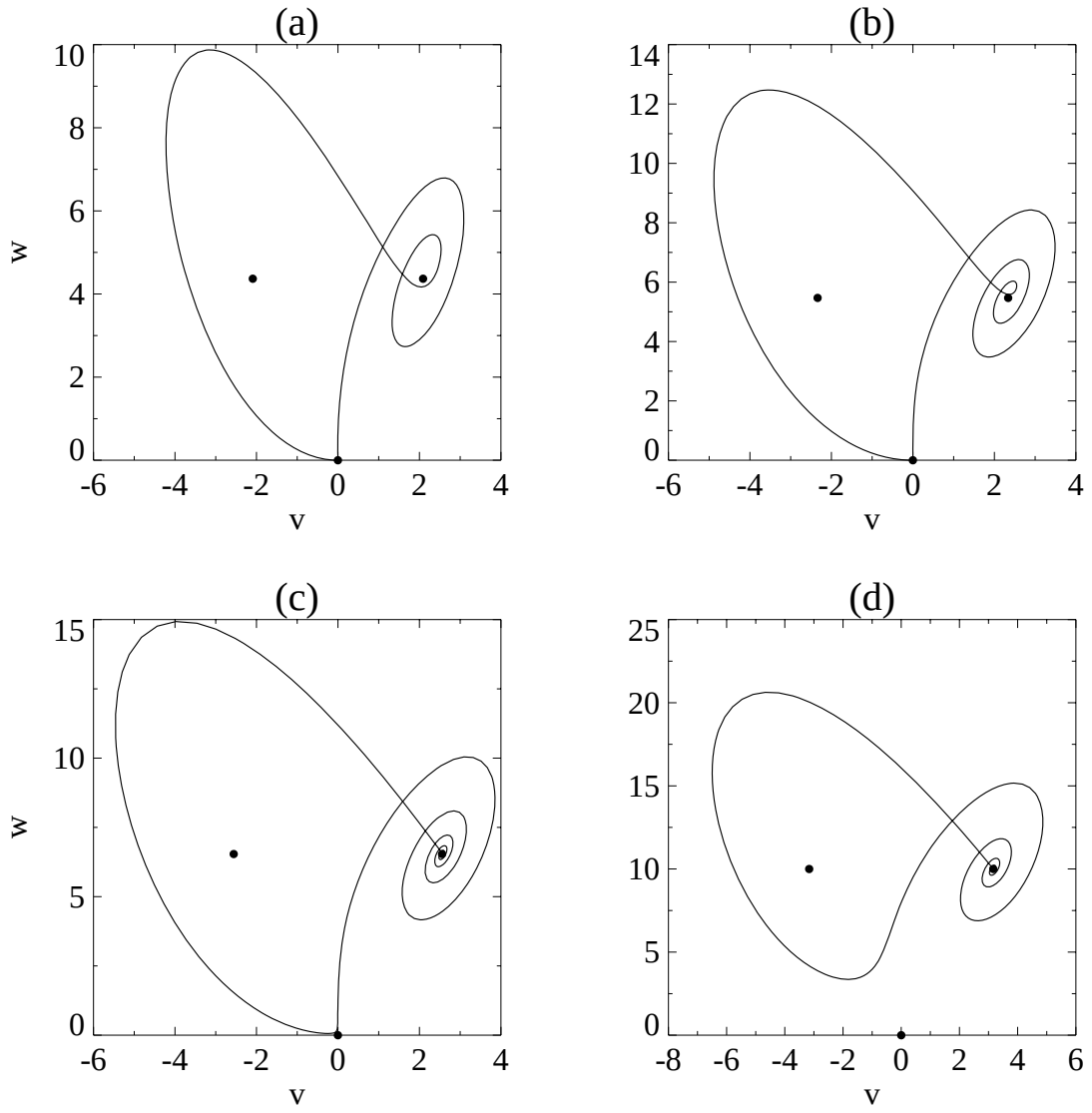

Figure 13. *Phase portraits of homoclinic orbits. (a) Homoclinic connection to the trivial solution, with* $(\kappa, \lambda) = (-1.5446, -4.3673)$. *(b) Homoclinic connection to the trivial solution, with* $(\kappa, \lambda) = (-1.7706, -5.4683)$. *(c) Near the heteroclinic connection between the trivial solution and a non-trivial equilibrium point, with* $(\kappa, \lambda) = (-1.9904, -6.5396)$. *(d) Homoclinic connection to the non-trivial equilibrium point, with* $(\kappa, \lambda) = (-2.1843, -10.0000)$. *The filled circles represent the three equilibrium points. For clarity, in each figure only one of the two connections is shown; the other one is related to the one shown by the reflection symmetry of the equations.*

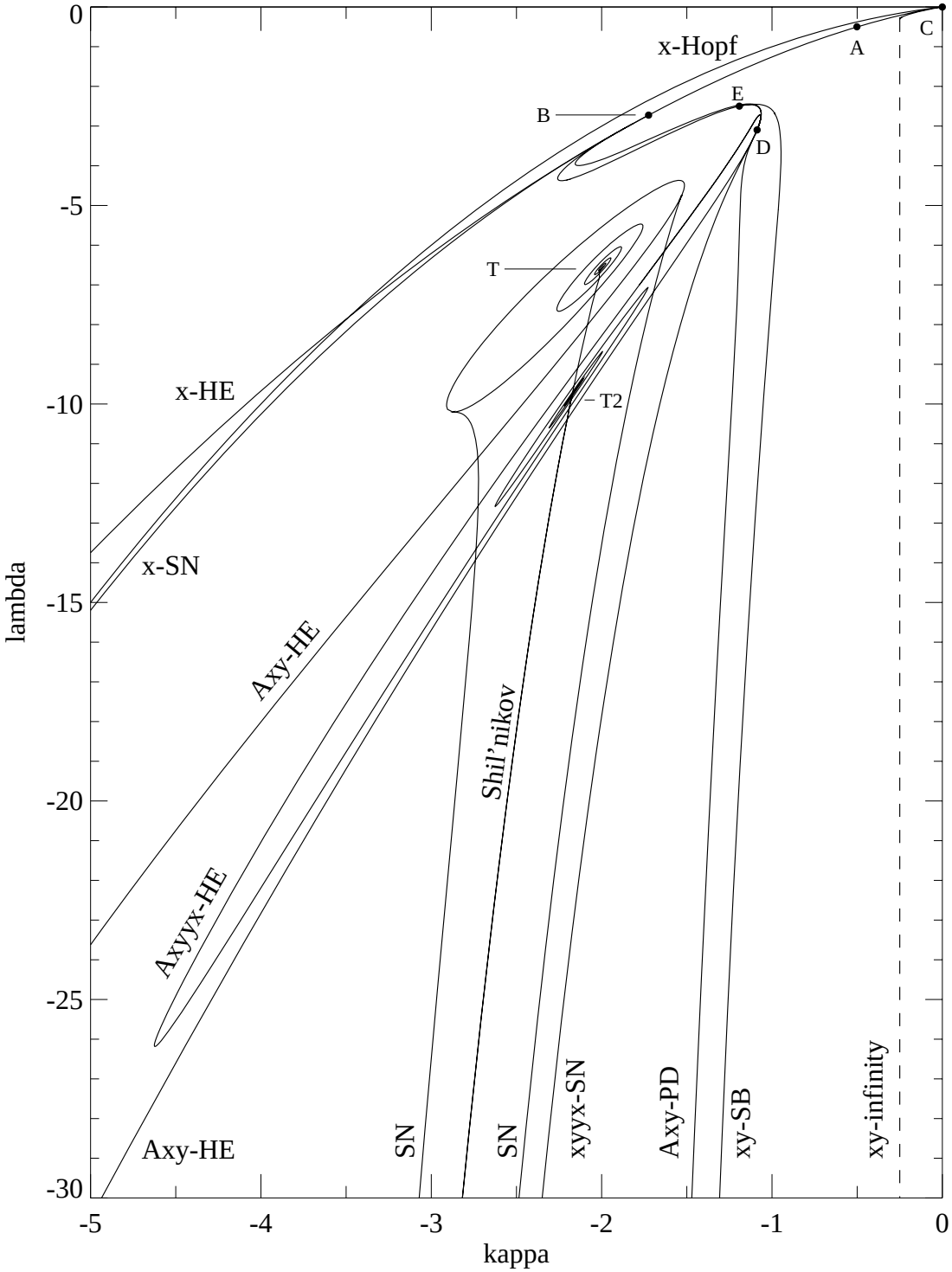

Figure 14. *Numerically computed unfolding diagram, including the bifurcation lines involved in the points T and T_2, which are at the centres of the two spirals (T is above T_2; the lower spiral is elongated). The two lines labelled SN indicate the first and second saddle-node bifurcations in the wiggles leading to the Shil'nikov bifurcation.*

studies of the PDEs governing magnetoconvection in narrow rolls are being carried out in an effort to find chaos created in a homoclinic explosion, as predicted by the ODEs [11]. Preliminary results indicate that the PDEs do have chaotic trajectories created in exactly the manner described in this paper over an appreciable range of roll widths.

The conditions necessary for the creation of chaotic trajectories of the type described here are met in other problems (for example, convection in a rotating layer [10] and the generalised Ginzburg–Landau equation [41]). The essential ingredient is a line of gluing bifurcations in the butterfly configuration crossing from $\delta > 1$ to $\delta < 1$. As described here, this occurs in two-dimensional convection in a vertical magnetic field provided that the aspect ratio of the rolls (ϖ) is small enough [11].

The constants M and N in (1) depend on the width of the rolls; in wider rolls, $M > 0$ and $N < 0$ [6], and the line of gluing bifurcations lies in the $\kappa \geq 0$ half-plane. This implies that at some point in the transition from narrow rolls to wider rolls, there is a codimension-three gluing bifurcation, at which the trivial solution has three eigenvalues of equal magnitude. At this bifurcation point, there is a simultaneous transition from the figure-of-eight to the butterfly configuration, and from gluing bifurcations to homoclinic explosions. Such a bifurcation point should be found in (3) (with the $\mathcal{O}(\varpi)$ corrections retained). With an even wider aspect ratio, we enter a régime where the constants M and N in (1) are opposite in sign to the case considered in this paper. In this régime, the homoclinic connections to the origin are replaced by heteroclinic connections between the nontrivial steady solutions; chaotic behaviour has been observed in this situation when the eigenvalues of the nontrivial solutions satisfy Shil'nikov's criterion [12, 13]. Thus magnetoconvection in rolls of variable aspect ratio would be a suitable system in which to study the transition from Lorenz-like chaos observed in this paper in narrow rolls ($\varpi \to 0$) to the period-doubling cascades associated with the Shil'nikov bifurcation in wider rolls.

Acknowledgements

During the course of this Advanced Research Workshop, I became aware of the work of Andrei Shil'nikov [21, 22, 23], who has analysed (2) independently and obtained similar results. I am indebted to him for several very stimulating conversations.

It is a pleasure to thank Nigel Weiss for his unfailing encouragement, and Keith Julien and Edgar Knobloch for many useful discussions. I also want to thank Paul Glendinning and Colin Sparrow for their helpful comments on the manuscript. I am grateful for support from the Commonwealth Scholarship and Fellowship Plan, from the Department of Applied Mathematics and Theoretical Physics, Cambridge and from Trinity College, Cambridge.

References

[1] M.R.E. Proctor and N.O. Weiss, Magnetoconvection, Rep. Prog. Phys. 45 (1982) 1317–1379.

[2] F. Takens, Forced oscillations and bifurcations, Comm. Math. Inst., Rijksuniversiteit Utrecht 3 (1974) 1–59.

[3] V.I. Arnol'd, Loss of stability of self-oscillations close to resonance and versal deformations of equivariant vector fields, Funct. Anal. Applic. 11 (1977) 1–10.

[4] J. Guckenheimer and P. Holmes, Nonlinear Oscillations, Dynamical Systems and Bifurcations of Vector Fields (Springer, New York, 1983).

[5] A. Arnéodo, P.H. Coullet, E.A. Spiegel and C. Tresser, Asymptotic chaos, Physica 14D (1985) 327–347.

[6] E. Knobloch and M.R.E. Proctor, Nonlinear periodic convection in double-diffusive systems, J. Fluid Mech. 108 (1981) 291–316.

[7] P.H. Coullet and E.A. Spiegel, Amplitude equations for systems with competing instabilities, SIAM J. Appl. Math. 43 (1983) 776–821.

[8] J. Guckenheimer and E. Knobloch, Nonlinear convection in a rotating layer: amplitude expansions and normal forms, Geophys. Astrophys. Fluid Dynamics 23 (1983) 247–272.

[9] E. Knobloch, On convection in a horizontal magnetic field with periodic boundary conditions, Geophys. Astrophys. Fluid Dynamics 36 (1986) 161–177.

[10] A.M. Rucklidge, Chaos in models of double convection, J. Fluid Mech. 237 (1992a) 209–229.

[11] A.M. Rucklidge, Chaos in magnetoconvection, (in preparation) (1992b).

[12] M.R.E. Proctor and N.O. Weiss, Normal forms and chaos in thermosolutal convection, Nonlinearity 3 (1990) 619–637.

[13] E. Knobloch and N.O. Weiss, Bifurcations in a model of magnetoconvection, Physica 9D (1983) 379–407.

[14] L.P. Shil'nikov, A case of the existence of a countable number of periodic motions, Soviet Maths. Dokl. 6 (1965) 163–167.

[15] E. Knobloch, N.O. Weiss and L.N. Da Costa, Oscillatory and steady convection in a magnetic field, J. Fluid Mech. 113 (1981) 153–186.

[16] E.N. Lorenz, Deterministic nonperiodic flow, J. Atmos. Sci. 20 (1963) 130–141.

[17] D.R. Moore and N.O. Weiss, Two-dimensional Rayleigh–Bénard convection, J. Fluid Mech. 58 (1973) 289–312.

[18] N.O. Weiss, Convection in an imposed magnetic field. Part 1. The development of nonlinear convection, J. Fluid Mech. 108 (1981a) 247–272.

[19] N.O. Weiss, Convection in an imposed magnetic field. Part 2. The dynamical regime, J. Fluid Mech. 108 (1981b) 273–289.

[20] T. Shimizu and N. Morioka, On the bifurcation of a symmetric limit cycle to an asymmetric one in a simple model, Phys. Lett. 76A (1980) 201–204.

[21] A.L. Shil'nikov, Bifurcations and chaos in the Morioka–Shimizu system (in Russian), in: Methods of Qualitative Theory of Differential Equations (Gorky State University, 1986) pp. 180–193. Published in English: Selecta Math. Sov. 10 (1991) 105–117.

[22] A.L. Shil'nikov, Bifurcations and chaos in the Morioka–Shimizu model: II (in Russian), in: Methods of Qualitative Theory of Differential Equations and Theory of Bifurcations (Gorky State University, 1989) pp. 130–138.

[23] A.L. Shil'nikov, On bifurcations of the Lorenz attractor in the Morioka–Shimizu model, these proceedings (1992).

[24] D.V. Lyubimov and M.A. Zaks, Two mechanisms of the transition to chaos in finite-dimensional models of convection, Physica 9D (1983) 52–64.

[25] T.S. Parker and L.O. Chua, Practical Numerical Algorithms for Chaotic Systems (Springer, New York, 1989).

[26] E. Doedel, AUTO: Software for Continuation and Bifurcation Problems in Ordinary Differential Equations (C.I.T. Press, Pasadena, 1986).

[27] C. Sparrow, The Lorenz Equations: Bifurcations, Chaos, and Strange Attractors (Springer, New York, 1982).

[28] P. Coullet, J.-M. Gambaudo and C. Tresser, Une nouvelle bifurcation de codimension 2: le collage de cycles, C. R. Acad. Sc. Paris 299 (1984) Série I, 253–256.

[29] A.M. Rucklidge, N.O. Weiss, D.P. Brownjohn and M.R.E. Proctor, Oscillations and secondary bifurcations in nonlinear magnetoconvection, Geophys. Astrophys. Fluid Dynamics (to appear) (1992).

[30] A.J. Rodríguez-Luis, E. Freire and E. Ponce, On a codimension 3 bifurcation arising in an autonomous electronic circuit, International Series of Numerical Mathematics 97 (1991) 301–306.

[31] P.A. Glendinning, Homoclinic bifurcations (Cambridge, Ph.D. thesis, 1985).

[32] D.V. Lyubimov, A.S. Pikovsky and M.A. Zaks, Universal scenarios of transition to chaos via homoclinic bifurcations, Sov. Sci. Rev. C. Math. Phys. 8 (1989) 221–292.

[33] J. Guckenheimer, A strange, strange attractor, in: The Hopf Bifurcation and Its Applications, eds. J.E. Marsden and M. McCracken (Springer, New York, 1976) pp. 368–381.

[34] A. Arnéodo, P. Coullet and C. Tresser, A possible new mechanism for the onset of turbulence, Phys. Lett. 81A (1981) 197–201.

[35] J. Coste and N. Peyraud, A new type of period-doubling bifurcations in one-dimensional transformations with two extrema, Physica 5D (1982) 415–420.

[36] V.V. Bykov, On the structure of the neighbourhood of the separatrix contour with a saddle-focus (in Russian), in: Methods of Qualitative Theory of Differential Equations (Gorky State University, 1978) pp. 3–32.

[37] P. Glendinning and C. Sparrow, T-points: a codimension two heteroclinic bifurcation, J. Stat. Phys. 43 (1986) 479–488.

[38] P. Glendinning and C. Sparrow, Local and global behaviour near homoclinic orbits, J. Stat. Phys. 35 (1984) 645–696.

[39] P. Gaspard, R. Kapral and G. Nicolis, Bifurcation phenomena near homoclinic systems: a two-parameter analysis, J. Stat. Phys. 35 (1984) 697–727.

[40] E. Knobloch, D.R. Moore, J. Toomre and N.O. Weiss, Transitions to chaos in two-dimensional double-diffusive convection, J. Fluid Mech. 166 (1986) 409–448.

[41] B.A. Malomed and A.A. Nepomnyashchy, Onset of chaos in the generalized Ginzburg–Landau equation, in: Nonlinear Evolution of Spatio-Temporal Structures in Dissipative Continuous Systems, eds. F.H. Busse and L. Kramer (Plenum Press, New York, 1990) pp. 419–424.

Chaos in a low-order model of magnetoconvection

A.M. RUCKLIDGE

Department of Applied Mathematics and Theoretical Physics,
University of Cambridge, Cambridge CB3 9EW, UK

Abstract

In the limit of tall, thin rolls, weakly nonlinear convection in a vertical magnetic field is described by an asymptotically exact third-order set of ordinary differential equations. These equations are shown here to have three codimension-two bifurcation points: a Takens–Bogdanov bifurcation, at which a gluing bifurcation is created; a point at which the gluing bifurcation is replaced by a pair of homoclinic explosions between which there are Lorenz-like chaotic trajectories; and a new type of bifurcation point at which the first of a cascade of period-doubling bifurcation lines originates. The last two bifurcation points are analysed in terms of a one-dimensional map. The equations also have a T-point, at which there is a heteroclinic connection between a saddle and a pair of saddle-foci; emerging from this point is a line of Shil'nikov bifurcations, involving homoclinic connections to a saddle-focus.

Keywords: Magnetoconvection, Shimizu–Morioka model, homoclinic bifurcations, Lorenz map, chaos.

Submitted to Physica D, August 1991, and in revised form May 1992. Proceedings of the NATO Advanced Research Workshop on Homoclinic Chaos, 6–9 May, 1991, Brussels.

Physica D **62** 323–337 (1993).